Computational Materials Science 124 (2016) 438–443

Contents lists available at ScienceDirect

Computational Materials Science

journal homepage: www.elsevier.com/locate/commatsci

Role of second-phase particle morphology on 3D grain growth: A phase-field approach

Kunok Chang *, Junhyun Kwon, Chang-Kyu Rhee

Korea Atomic Energy Research Institute, 989-111 Daedeok-daero, Yuseong-gu, Daejeon 34057, Republic of Korea

ARTICLE INFO

Article history:
Received 4 June 2016
Received in revised form 10 August 2016
Accepted 11 August 2016
Available online 28 August 2016

Keywords:
Grain growth
Zener pinning
Phase-field modeling

ABSTRACT

The incorporation of second-phase particles in polycrystalline materials is one of the most efficient and practical methods for the retardation of grain growth during high-temperature heat treatment. To obtain a more systematic understanding of the related pinning effect, we employ a multi-order-parameter phase-field grain-growth model to simulate 3D grain growth in the presence of inert second-phase particles. We compare the pinning efficacy of the second-phase particles depending on the particle size, distribution, morphology, and the number of alignment directions. The dependence of the number of average neighboring grains on the spatial distributions of the inert second-phase particles is also evaluated.

© 2016 Elsevier B.V. All rights reserved.

1. Introduction

The prevention of grain growth during high-temperature heat treatment is quite important for the retention of sufficiently high material strength [1–4]. Because of the significance of Zener pinning, particle pinning has been widely investigated using not only experimental approaches [1–4], but also analytical [5–9] and numerical [10–17] methods.

Approximately 70 years ago, Zener and Smith proposed an analytic theory indicating that a pinning force is generated by a spherical particle via the isotropic particle/matrix interfacial energy [5]. Their significant achievement was then extended to the ellipsoidal particle case, where the particle makes contact with the grain boundary at a right angle, by Nes et al. [8]. Subsequently, the right-angle assumption was relaxed by Ringer et al. [9], and the pinning force generated by a single ellipsoidal particle was reevaluated numerically by Chang and Chen [16]. Further, Chang et al. evaluated the role of the particle morphology using phase-field modeling for multiparticles and multigrains in two dimensions (2D) [10], and for a single grain boundary and a particle in three dimensions (3D) [16], under the assumption that the grain boundary meets the particle at a right angle.

However, this assumption is not necessarily true in reality; therefore, a more generalized analysis is required in order to estimate the pinning effect dependence on the particle morphology. For example, the oxide particle morphology in oxide-dispersion-strengthened (ODS) steel ranges from spherical to cubic/cuboidal particles [18]. Therefore, to predict the mechanical properties of Fe-ODS steel, it is important to evaluate the pinning force applied by both the cuboidal and cubic particles.

In this study, we perform 3D grain-growth phase-field modeling to investigate the effects of the particle size distribution and particle morphology on the pinning efficiency. In their paper, Chang and Chen [16] measured the pinning force applied by a single ellipsoidal and cubic particle using the phase-field method in 3D; here, we extend this work to a polycrystalline system with multiple particles. We also investigate the effects of the spherical-particle size distribution, the particle morphology (spherical/cubic), and the particle direction variance (1-, 3-, 9-direction-aligned cubic particles) using phase-field modeling. In the previous study conducted in 2D [10], the effect of the particle size distribution was negligible. In contrast, the spherical-particle size distribution cannot be neglected in the 3D case, and its influence on the pinning efficiency is investigated in this study.

2. Simulation details

2.1. Phase-field model for grain growth with inert second-phase particles

We adopt the multi-order-parameter grain-growth model proposed by Chen and Wang [19]. In this setup, the crystallographic orientations of the single-phase polycrystalline materials are represented by the set of non-conserved order parameters:

* Corresponding author.
E-mail address: kunokchang@kaeri.re.kr (K. Chang).

http://dx.doi.org/10.1016/j.commatsci.2016.08.019
0927-0256/© 2016 Elsevier B.V. All rights reserved.

$$\eta_1(\mathbf{r},t),\ \eta_2(\mathbf{r},t),\ldots,\eta_Q(\mathbf{r},t), \tag{1}$$

where η_i $(i=1,2,\ldots,Q)$ are the non-conserved order parameters, $\mathbf{r}$ is the position vector, and t is time. Assuming that the total number of order parameters is Q, we simply evolve P-order parameters $(P<Q)$ only during the simulations [10]. The parameters represent the grains while remaining constant during the simulations $(Q-P)$ so as to describe inert second-phase particles (precipitate).

The relaxation of the η_i is governed by the Ginzburg-Landau time-dependent equations for each η_i, where

$$\frac{\partial\eta_i(\mathbf{r},t)}{\partial t}=-L_i\frac{\delta F}{\delta\eta_i(\mathbf{r},t)},\qquad i=1,2,\ldots,Q, \tag{2}$$

Further, the total free energy function F is expressed as

$$F=\int_V\left[\sum_i^Q\left(\frac{\eta_i^4}{4}-\frac{\eta_i^2}{2}\right)+\gamma\sum_i^P\sum_{i\neq j}^Q\eta_i^2\eta_j^2+\frac{\kappa_i}{2}\sum_i^Q(\nabla\eta_i)^2\right]dV. \tag{3}$$

We substitute Eq. (3) into Eq. (2) to obtain

$$\frac{\partial\eta_i(\mathbf{r},t)}{\partial t}=-L_i\left(-\eta_i+\eta_i^3+2\gamma\eta_i\sum_{j=1}^P\eta_j^2-\kappa_i\nabla^2\eta_i\right),\qquad i=1,2,\ldots,Q. \tag{4}$$

2.2. Numerical schemes and parameters

To eliminate the early-stage non-physical grain coalescence and to improve the computational efficiency, we adopt the active parameter tracking algorithm [20]. Further, to discretize the time derivative in Eq. (4), we adopt the forward-Euler discretization scheme

$$\eta_i(t+\Delta t)=\eta_i(t)+\frac{d\eta_i}{dt}\Delta t+O(\Delta t). \tag{5}$$

We assume that the error term $O(\Delta t)$ is negligible in our simulations. The phenomenological parameters in Eqs. (2)–(4) are set to $L_i=\gamma=1.0$ and $\kappa_i=0.5$ in our simulations. All interfacial energy is isotropic and the interface width is 3 grid points and the energy is 0.24 (a/u). The gradient coefficient is chosen to be relatively low compared to those of former studies [11,16,19], so that the grain boundary motion can be retarded more easily. Further, $\nabla^2\eta_i$ in Eq. (4) is evaluated as

$$\nabla^2\eta_i(\vec{r})=\sum_{j=1}^6[\eta_i(\vec{r_j})-\eta_i(\vec{r})]/(\Delta x)^2, \tag{6}$$

where the $\vec{r_j}$ terms represent the first-nearest neighbor positions of $\vec{r}$ and Δx is the change in position on the x-axis. We set $\Delta t=0.1$ in Eq. (5) and $\Delta x=1.0$ in Eq. (6) and apply a periodic boundary condition in the x, y, and z directions. The simulation cell has 600^3 grid points and 90,000 initial grains are randomly distributed. The initial radius of each grain is 6.0 grid points and no overlap between grains is permitted. We conducted 12-nodes parallel computing (Message Passing Interface) to obtain a large-scale grain structure within a reasonable time frame (approximately 12 days).

3. Simulation results

3.1. Structures with homogeneous spherical particles

As the grain growth proceeds, the number of grains decreases and the average grain diameter d_g increases, as shown in Figs. 1 and 2. A structure having a 5% volume fraction of second-phase spherical particles with radius $r=8.1$ grid points is shown in Fig. 3. As mentioned in the Introduction, the second-phase particles play an effective role in hindering grain growth; thus, the d_g in Fig. 3 is notably smaller than that of the structure in Fig. 2. For comparison, the d_g values are plotted as a function of time for a structure without second-phase particles ("particle-free") and for structures having particles with $r=5.7$, 8.1 and 10.5 grid points in Fig. 4.

In a previous 2D study [10], frozen grain structures produced by second-phase particle pinning were obtained and it was possible to evaluate the pinned grain size. However, as the grain boundary is

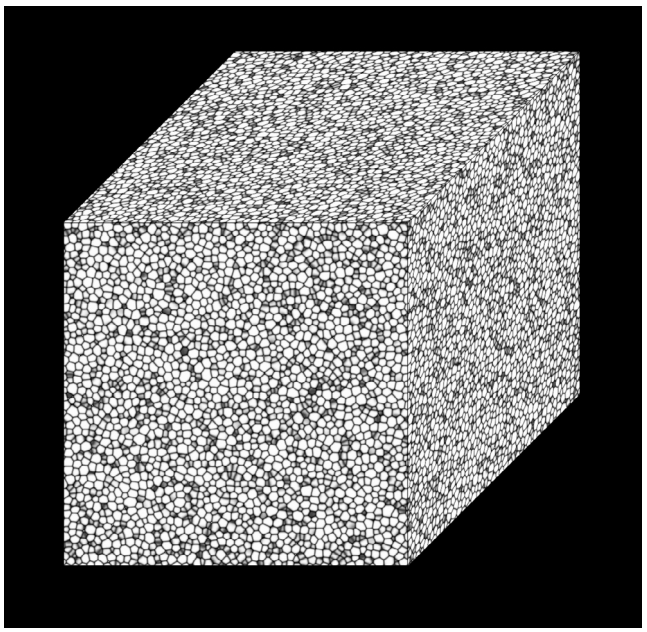

Fig. 1. 3D microstructure generated via phase-field grain-growth simulation on 600^3 cubic grid. The microstructure is visualized through mapping of the squared-order parameter values onto a gray palette. At 1000 time steps ($\Delta t=0.1$), 90,000 grains having an average grain diameter d_g of 16.31 are obtained.

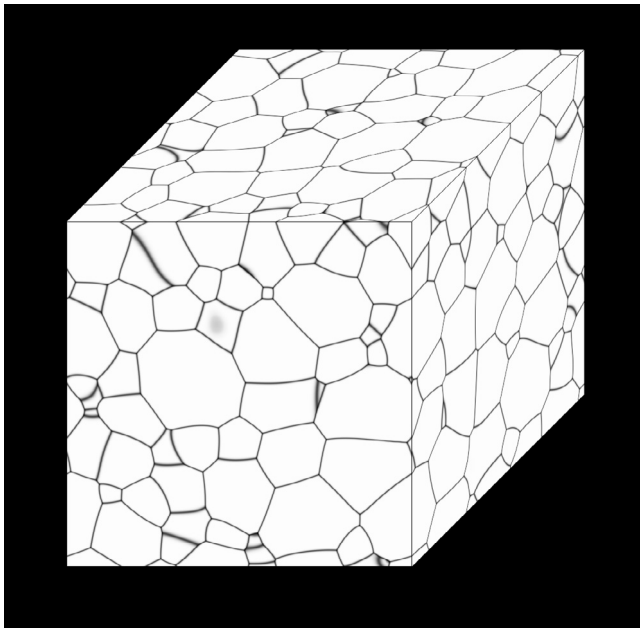

Fig. 2. 3D microstructure generated via phase-field grain-growth simulation on 600^3 cubic grid. The microstructure is visualized through mapping of the squared-order parameter values onto a gray palette. At 90,000Δt , 312 grains having a d_g of 97.04 are obtained.

Download English Version:

https://daneshyari.com/en/article/1559812

Download Persian Version:

https://daneshyari.com/article/1559812

Daneshyari.com